Metals and Materials International (2022) 28:755–769
https://doi.org/10.1007/s12540-020-00917-0

Effect of Homogenisation Temperature on the Microstructure and Microhardness of As-Cast H13 Steel

Yahui Han[1] · Changsheng Li[1] · Shuai He[1] · Cairu Gao[1] · Shuaishuai Chen[1] · En Li[1]

Received: 2 September 2020 / Accepted: 29 October 2020 / Published online: 19 January 2021

Abstract
This study determined that the homogenisation temperature range of experimental as-cast H13 steel was from 1150 to 1230 °C, whilst the effect of homogenisation temperature range on the microstructural evolution and microhardness was tested. The enrichment of alloying elements in the dendrite segregation region decreased the solidus temperature of matrix, whose total content determined the maximum homogenisation temperature. The secondary dendrite branches were most dissolved at 1150 °C, and overheating appeared at 1230 °C in the segregation region. Moreover, the primary carbides underwent shrinking, passivation, fragmentation and dissolution. The secondary carbides $M_{23}C_6$ and M_6C were formed at the interfaces of MC/γ and M_7C_3/γ, respectively. As the homogenisation temperature increased from 1150 to 1230 °C, the value of microhardness gradually decreased from 771 to 740 HV. Nevertheless, the standard deviation value decreased first and then increased, which reached the minimum 32 HV at 1200 °C, indicating that the hardness homogeneity was the best.

Keywords As-cast H13 steel · Homogenisation temperature · Dendrite segregation · Primary carbide · Microhardness

1 Introduction

Hot-working die steels are broadly applied to make die for hot deformation of metals, such as hot forging die, hot extrusion die and hot upsetting die [1, 2]. Under high temperature and high-pressure conditions, the die materials are required to have high thermal strength, high hardness and high thermal stability [3]. AISI H13 steel is the traditional and common hot-working die steel around the world [4]. This steel contains about 0.40 wt% carbon and a total of 8 wt% alloying elements (chromium, molybdenum and vanadium), which ensures its excellent mechanical properties. However, owing to the non-equilibrium solidification, the solidification structure of H13 steel presents an obvious dendrite morphology, in which the element segregation and primary carbides are widely distributed [5]. Dendrite segregation and primary carbides will deteriorate the hot workability and toughness [2, 6]; therefore, it is necessary for H13 steel to alleviate dendrite segregation and eliminate primary carbides. In traditional industries, the common method is a high-temperature homogenisation treatment [7, 8], which depends on the homogenisation temperature and soaking time. The effect of soaking time on the as-cast H13 steel has been previously reported [9]; the effect of homogenisation temperature is investigated in this work. The alloying elements diffuse from the interdendritic region to the neighboring dendrite arm region and the dendrites are gradually eliminated. The dendrite dissolution during homogenisation is a matter of mass transport, whose rate varies with the homogenisation temperature. It is significant to study the dendrite dissolution behavior at different homogenisation temperatures. Furthermore, most of the primary carbides in as-cast H13 steel dissolve in the matrix after homogenisation and the residual will affect the performance [10]. Ning et al. [11] reported that the precipitates in H13 steel were V_8C_7

✉ Changsheng Li
lics@ral.neu.edu.cn

Yahui Han
hui120612han@163.com

Shuai He
1519762189@qq.com

Cairu Gao
gaocr@ral.neu.edu.cn

Shuaishuai Chen
2722306400@qq.com

En Li
lien977@163.com

[1] State Key Lab of Rolling and Automation, Northeastern University, Shenyang 118019, People's Republic of China

(as-cast state), $Cr_{23}C_6$ (annealed state) and $Cr_3C_2(Cr_2VC_2)$ (tempered state). Wang et al. [12] reported that primary carbides M(C, N), M_6(C, N) and M_7C_3 precipitated in an ingot. M_6(C, N) and M_7C_3 were almost dissolved and M(C, N) were partially dissolved. Finally, smaller size primary M(C, N) existed in the quenched and tempered H13 steel. Song et al. [13] reported the primary carbides V_8C_7 and Fe_3Mo_3 were partially dissolved after homogenisation. These investigations just revealed the final states of the primary carbides in as-cast H13 steel after homogenisation treatment. The evolution mechanism of primary carbides during homogenisation is still not clear.

The homogenisation treatment must be carried out in the safe temperature range. At present, a common practice to decide the range of homogenisation temperature in the literature is to calculate 0.9 T_m to 0.95 T_m, where T_m is the melting temperature [14]. However, it is generally believed that the homogenisation temperature is between 1200 and 1300 °C for H13 steel [15, 16]. Given that the solute segregation always lowers the local solidus temperature in the dendrite region, the local melting is likely to occur in the severe dendrite segregation region or around primary carbides [17]. Furthermore, different metallurgical qualities of ingots would undergo a different homogenisation progress and attain different final states even when treated with the same homogenisation process. For example, the microstructure and properties of electro-slag H13 steel and electric furnace H13 steel were comparatively studied by Wang et al. [18], who found that band segregation of the electric furnace steel was more serious with the same production technology. The high-temperature behaviour of primary carbide in as-cast H13 steel under different solidification conditions was studied by Mao et al. [19]; compared to electro-slag ingots, the area of local liquid phase around the carbide in electric furnace ingot was larger when heated at the same temperature. Therefore, it is essential to determine the homogenisation temperature range first for as-cast H13 steel.

In this work, a type of as-cast H13 steel was designed and manufactured by vacuum induction melting in the laboratory. The microstructure and microhardness in relation to the homogenisation temperature were investigated and the optimised homogenisation temperature range based on the experimental measures and solidus temperature theoretical calculation were proposed.

2 Experimental Procedure

2.1 Material

The as-received H13 steel used in this study was prepared by vacuum induction melting in the laboratory, which was smelted at 1530 °C and casted at 1450 °C. The size of the chill cast ingot was 390 mm in length with a diameter of 160 mm, the taper angle of casting die was set to 2° to facilitate the ejection. Based on the NADCA #207-2003 standard [4], the chemical composition was represented as, 0.40, C-0.89, Si-0.42, Mn-1.01, V-5.15, Cr-1.74 wt% Mo; the other elements P, S and N each had a concentration of less than 0.02 wt%.

2.2 High-Temperature Homogenisation Treatment Process

Soaking time is an essential parameter of the homogenisation process. The effect of soaking time has been studied by previous work [9], which suggested that more than 20 h at 1200 °C were required to attain the homogenised state. This work aims to optimise the homogenisation temperature range and reveal the corresponding microstructural changes. Therefore, a long soaking time is not necessary, but it requires taking a certain amount of time to achieve a certain homogenisation degree. The required minimum soaking time of different size specimens was set with the Eq. (1),

$$\tau = K * \alpha D \tag{1}$$

where τ is the soaking time, K is correction factor (selection for 1.0–1.3), α is heating coefficient (0.7–0.8 min/mm) and D is effective workpiece thickness. The homogenisation specimens were machined from the columnar crystal region of the experimental ingot. Two homogenisation treatment series were designed.

1. High-temperature homogenisation *in-situ* observations were conducted by a confocal laser scanning microscopy (CLSM) to observe the real-time microstructural evolution. Each surface of cylindrical specimens with the dimension of Φ 5 × 4 mm was polished, and high purity argon gas was passed through the specimen chamber to prevent surface oxidation during homogenisation. The heating processes (P1–P6) are schematically shown in Fig. 1. The P1 in Fig. 1a was a continuous heating process to observe the real-time dendrite change with the increase of homogenisation temperature to analyse the required minimum homogenisation temperature. In the meantime, a heat preservation stage at each homogenisation temperature was set for the diffusion of segregated elements. The specimen was gradually heated up to the specific temperature (850, 1100, 1150 and 1200 °C) at the heating speed of 0.1 °C/s, and the specimen was separately kept for 300 s at a specific temperature. In Fig. 1b, temperatures (1150, 1200, 1230, 1250 and 1280 °C) were set to decide the upper limit of the homogenisation temperature; the specimens were all first heated up to 850 °C at 0.1 °C/s and held for 300 s,

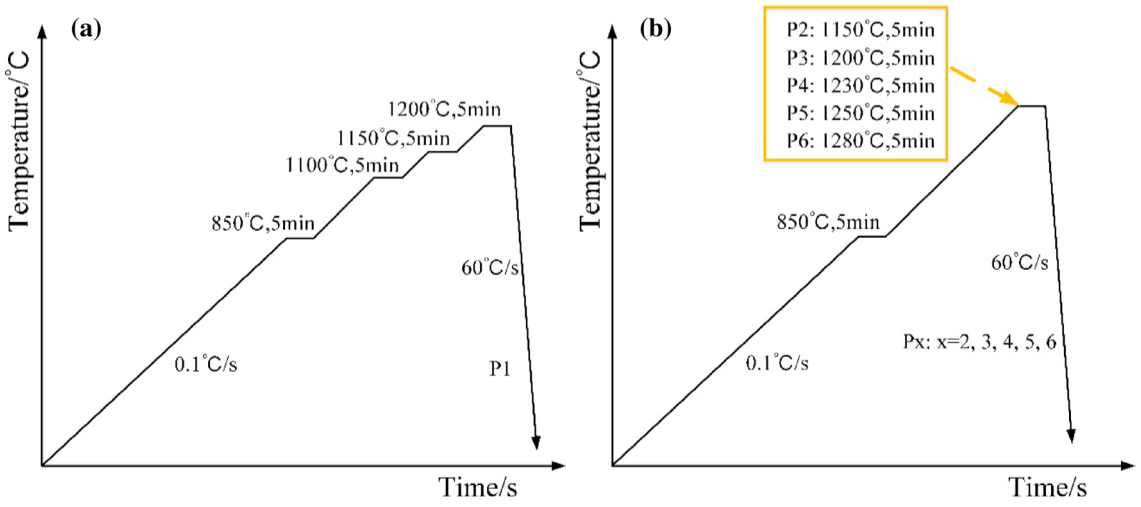

Fig. 1 Diagram of homogenisation process: **a** P1 and **b**P2, P3, P4, P5 and P6

then they were heated up to the specific peak temperature at 0.1 °C/s and held for 300 s. Using helium as a coolant and controlling the blowing speed, the specimens could be cooled to room temperature at 60 °C/s to preserve the microstructure at high temperature.

2. The specimens with dimension of 10 × 10 × 10 mm were homogenised in an electric furnace; argon was also charged to prevent the surface oxidation of the specimens. After the homogenisation treatment, the homogenised specimens were immediately water quenched to room temperature. The homogenisation temperatures of 1100, 1150, 1200 and 1230 °C were selected. The soaking time was 30 min, more than the required time of 10 min, to attain a certain homogenisation degree.

2.3 Microhardness Test

High-temperature homogenisation treatment can help to the reduction of dislocations and dendrite segregation generated by the non-equilibrium solidification, which affects the microhardness of homogenised H13 steel. The microhardness tester was applied to obtain the microhardness values of homogenised specimens, and the load applied was 200 g. Ten points were tested across the segregation region of the homogenised specimens. The mean value and standard deviation value were adopted to achieve the microhardness value and characterise the homogeneity degree after homogenisation treatment.

2.4 Methods of Microstructure Analysis

The microstructural observation specimens were handled by standard mechanical grinding and polishing, and then etched with 5% nitric acid. The microstructural morphology was analysed by a BX53MRF OLYMPUS optical microscopy (OM) and a QUANTA 600 scanning electron microscopy (SEM). The energy dispersive spectrometer (EDS) analysis was done by an OXFORD INCA X-Act energy dispersive spectroscope equipped on the scanning electron microscope; the resolution was 130 eV. The elemental map scanning was conducted on a JEOL JXA 8530F electron probe. The X-ray diffraction (XRD) specimens were also handled by standard mechanical grinding, followed by electrochemical polishing in a solution of 10% $HClO_4$ in alcohol at 20 V for 18 s. The XRD tests were conducted on a D8 DISCOVER X-ray diffractometer with a Cu-target; the scanning speed was 2°/min in the scanning range of from 30° to 90°. Thin foil specimens for transmission electron microscope (TEM) observation (FEI Tecnai G2 F2) were prepared by electrochemical polishing at − 32 °C for 20 s in a solution containing 10% perchloric acid and 90% methanol. For the preparation of the carbon replicas, the homogenised sample was first mechanical ground and polished, and then chemically etched in a solution of 5% HNO_3 in distilled water. After evaporating the carbon onto the etched surface of a sample, the scratched carbon films were floated to the surface using a solution of 10% HCl in methanol and an applied voltage of 2 V at 20 °C. Finally, the carbon films were picked up with copper mesh and dried for TEM observation.

3 Experimental Results

3.1 Solidification Microstructure Characterisation

The as-cast structure is listed in Fig. 2a, it presented the dendrite segregation morphology and contained primary carbides in the dendrite segregation region. The carbide

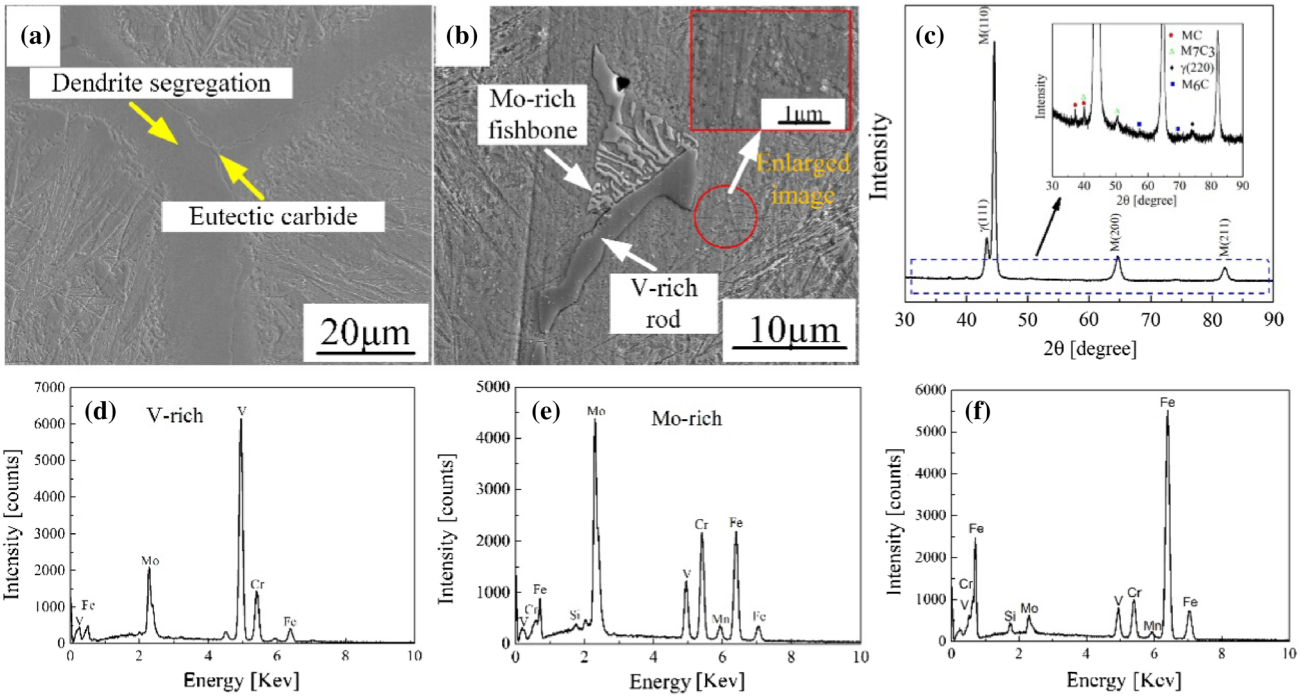

Fig. 2 Solidification structure: **a** secondary electron image; **b** carbide morphologies under secondary electron of SEM and **c** as-cast XRD spectrum. EDS spectra of carbides: **d** V-rich rod-like; **e** Mo-rich plate-like and **f** dot-like

morphologies were rod-like, plate-like and dot-like, as shown in Fig. 2b. The corresponding EDS spectra of different carbide morphologies in Fig. 2b are plotted in Fig. 2d–f, respectively; note the coexisted primary V-rich (rod-like) and Mo-rich (plate-like) carbides under the as-cast state. The applied acceleration voltage during measurement was about 40 keV, the interaction volume between the electron beams was bigger than the dot-like carbide size. Consequently, the EDS spectra in Fig. 2f was a mixture of dot-like carbides and the surrounding matrix. The XRD analysis in Fig. 2c shows that the matrix phase under the as-cast state was martensite (BCT), accompanied with retained austenite and carbide. The carbide constituent was comprised primarily of MC and M_7C_3. Vanadium strongly promoted the formation of MC-type carbides and the formation of metastable M_7C_3-type carbides containing a high content of molybdenum and chromium could be attributed to the non-equilibrium solidification [20]. The diffraction peaks at 44.2° and 74.2° are the (111) and (220) plane of retained austenite. The fraction of carbides was small and their diffraction intensity was weak; the diffraction intensity of M_6C carbides was so weak that its peak was not distinct when compared to that of M_7C_3 and MC. Referring to PDF card 89-4884 and a previous report [12], the M_6C position of reflection located at 58.4° and 68.6°.

3.2 Homogenisation Temperature Range

The elemental diffusion at a lower temperature is slow during homogenisation, as such the required soaking time is long. Therefore, the critical homogenisation temperature is necessary to be determined. The heat-treatment process is detailed in P1 in Fig. 1 and the corresponding results of the confocal laser scanning microscopy are shown in Fig. 3. Owing to the thermal corrosion effect, the phase with different elemental concentration will have the contrast differences at high temperature. Consequently, the elemental segregation regions can be recognised. The elemental segregation is visible when the temperature increased to 850 °C in Fig. 3a, which is the atypical dendrite morphology. The grain is visible in Fig. 3b when it reached 1100 °C and the elemental segregation regions on the matrix still exist. With the increase of homogenisation temperature, the grain size becomes larger and the elemental segregation regions in the same position almost disappear in Fig. 3c, indicating the diffusion process in elemental segregation regions will be enhanced when the homogenisation temperature was 1150 °C. It has little effect on grain size and elemental segregation in the same position in Fig. 3d at 1200 °C. In conclusion, the elemental segregation regions still existed after homogenisation at 1100 °C for 300 s, and the diffusion

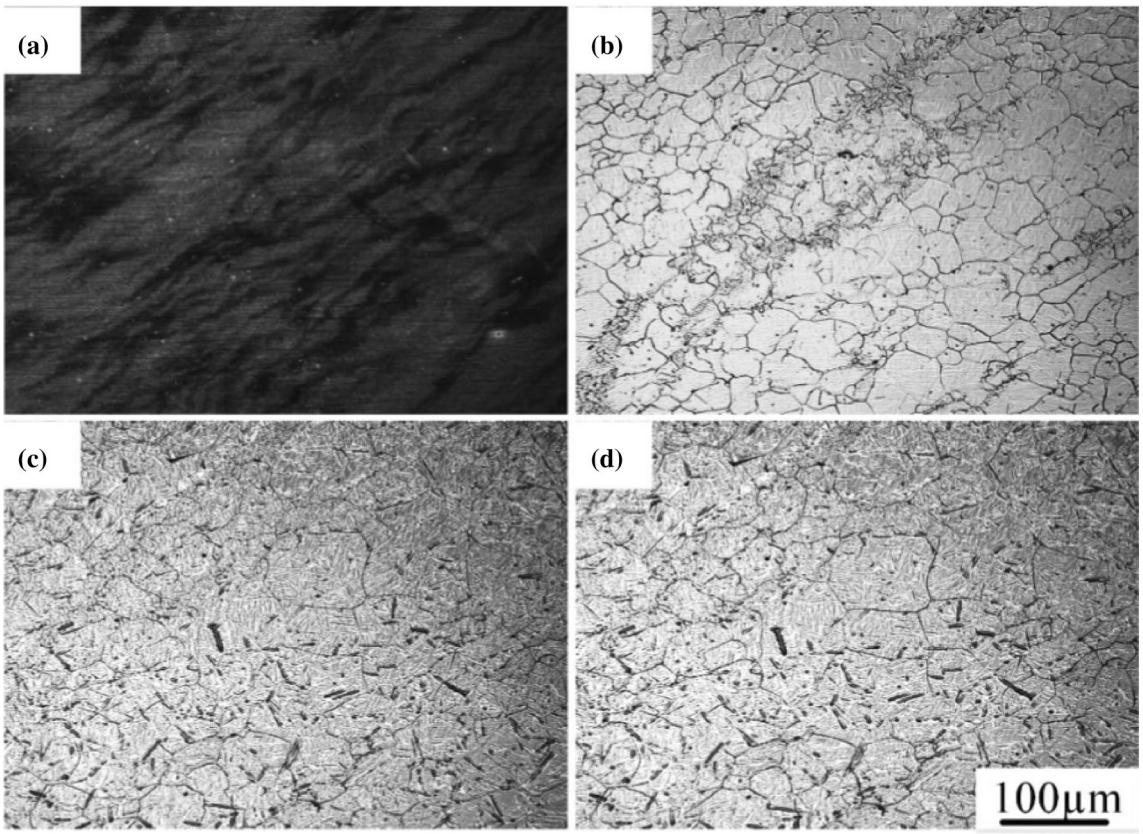

Fig. 3 Optical images at different isothermal holding temperature in process 1: **a** 850 °C; **b** 1100 °C; **c** 1150 °C and **d** 1200 °C

efficiency decreased with the decrease of the concentration gradient, indicating more than 300 s was required to eliminate the residual elemental segregation when the homogenisation temperature was 1100 °C. The residual elemental segregation was almost eliminated after homogenisation at 1150 °C for 300 s, and there were no changes when the homogenisation temperature increased to 1200 °C. Therefore, the critical homogenisation temperature was 1150 °C.

As proposed in previous work, the soaking time decreases with the increase of homogenisation temperature [9], indicating the diffusion process is enhanced at a higher temperature. However, the elemental segregation in the interdendritic region will decrease the solidus temperature, thus leading to the decrease of the upper limit of homogenisation temperature. To study the upper-temperature limit and microstructural evolution when the homogenisation temperature is over 1200 °C, temperatures of 1150, 1200, 1230, 1250 and 1280 °C were selected. The microstructural evolution at 1150 and 1200 °C served as contrasts. Some representative results are listed in Fig. 4. In P3, as the temperature increased to 1200 °C, the segregated elements and carbide particles gradually dissolved into the matrix. After soaking for 300 s, the carbides along the grain boundary became discontinuous. Eventually, it exhibits a more uniform structure (Fig. 4c). When the homogenisation temperature was 1230 °C, stable overheating appeared, as indicated by the red arrows, the grain boundaries bulge and present the gap state (Fig. 4e). Overburning appeared when the homogenisation temperature increased to 1250 °C, and local melting occurred around the grain boundaries (Fig. 4h). In addition, the overheating and overburning features became more serious after heat preservation (Fig. 4f, i). The overheating and overburning deteriorated the grain boundary binding force and the hot-working character of the ingot. Therefore, the upper limit of the homogenisation temperature is 1230 °C.

3.3 As-cast Microstructure

3.3.1 Evolution of Dendrite Structure

As described in Sect. 3.2, the as-cast structure went through a significant change when the homogenisation temperature increased from 1100 to 1230 °C. The dendrite segregation was gradually eliminated, and overheating appeared when homogenisation temperature was 1230 °C. Therefore, the homogenisation temperature range (1150–1230 °C) was selected. To observe the evolution of dendrite structure in the temperature range, the

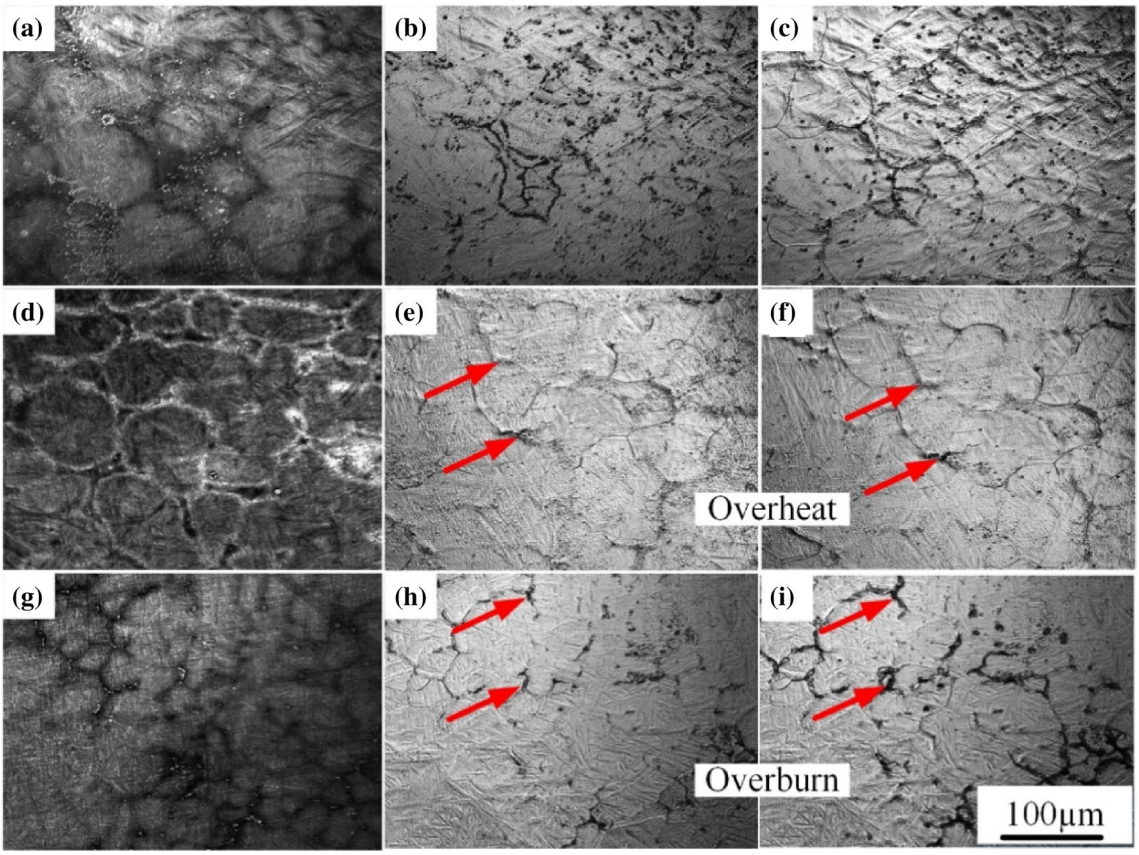

Fig. 4 Evolution of microstructure in different heating processes: P3 **a** 850 °C →, **b** 1200 °C →, **c** 1200 °C -300 s; P4 **d** 850 °C →, **e** 1230 °C →, **f** 1230 °C -300 s; P5 **g** 850 °C →, **h** 1250 °C →, **i** 1250 °C -300 s

homogenisation treatments with an electric furnace were carried out and a homogenisation temperature of 1100 °C was set as a contrast. The corresponding dendrite evolution in the temperature range is exhibited in Fig. 5. The dendrite had the largest density at 1100 °C and the dendrite was still existed at temperature of 1230 °C. The overall variation trend of dendrite density was downward from 1100 to 1230 °C. The secondary dendrite branches were mostly eliminated when the specimen was homogenised at 1150 °C (Fig. 5b), which also indicates that the critical homogenisation temperature should be 1150 °C. Also, the proportion of inter-dendritic region increased when the homogenisation temperature increased to 1200 °C. This illustrated that the movement of atoms from high concentration region to low concentration region increased the area of inter-dendritic region. Whilst the concentration gradient gradually decreased due to the element diffusion; thus, the stability of undercooled austenite and the content of retained austenite after water quenching in dendrite segregation regions were reduced. In addition, the overheating appeared in the segregation region at 1230 °C and the grains coarsened with the increase of homogenisation temperature, as expected.

3.3.2 Evolution of Interdendritic Carbide

Generally, there are a certain amount of interdendritic primary carbides in as-cast H13 steel, which will inevitably dissolve in the matrix during homogenisation. The morphologies of primary carbides at different homogenisation temperatures are listed in Fig. 6. As the homogenisation temperature increased from 1100 to 1230 °C, the primary carbides underwent shrinking (transforming from section to point), passivation, fragmentation and dissolution [21, 22], as indicated by the red arrows. Finally, the massive primary carbides were almost dissolved at 1230 °C (Fig. 6d). The obscured grain boundaries appeared in the interdendritic region, as indicated by the green arrows in Fig. 6c.

As illustrated in Sect. 3.1, the coexisted primary V-rich (MC) and Mo-rich (M_7C_3) carbides exist in as-cast H13 steel. Generally, primary carbides in as-cast H13 steel are thermodynamically metastable and will go through decomposition and dissolution during homogenisation. Figure 7 shows the morphologies of primary carbides at different homogenisation temperatures; there are decomposition zones around primary carbide at 1100 and 1150 °C, where many black and grey granular phases were observed at the

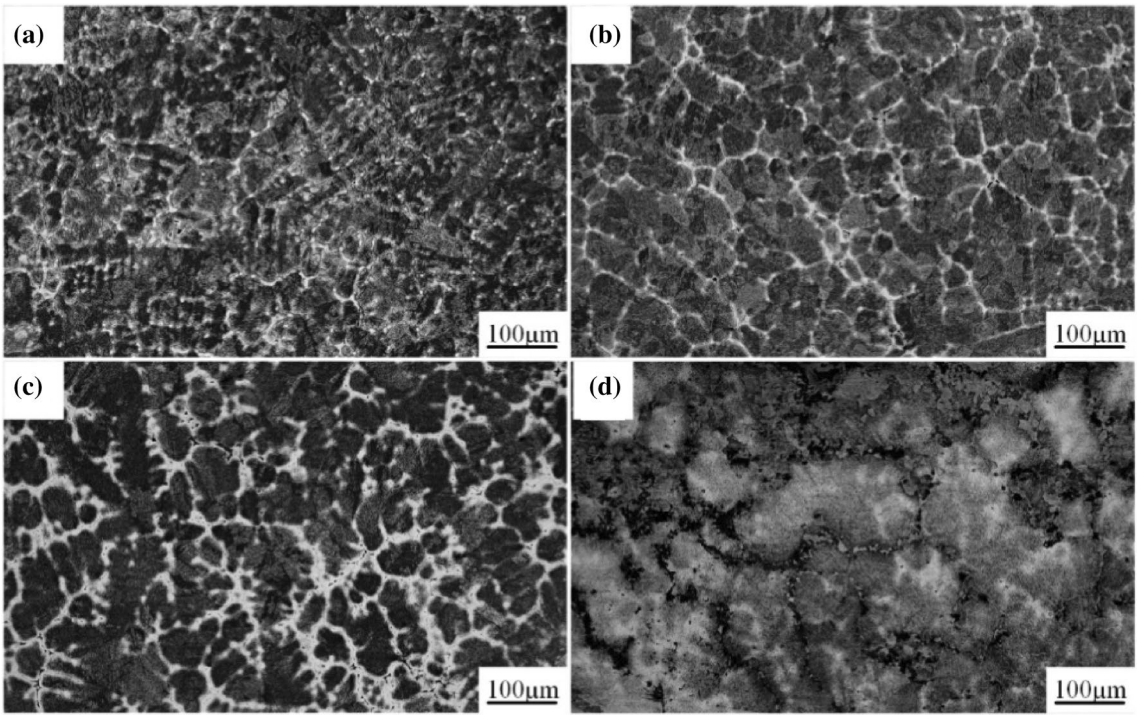

Fig. 5 Optical micrographs at different soaking temperature for 30 min in homogenisation process: **a** 1100 °C; **b** 1150 °C; **c** 1200 °C and **d** 1230 °C

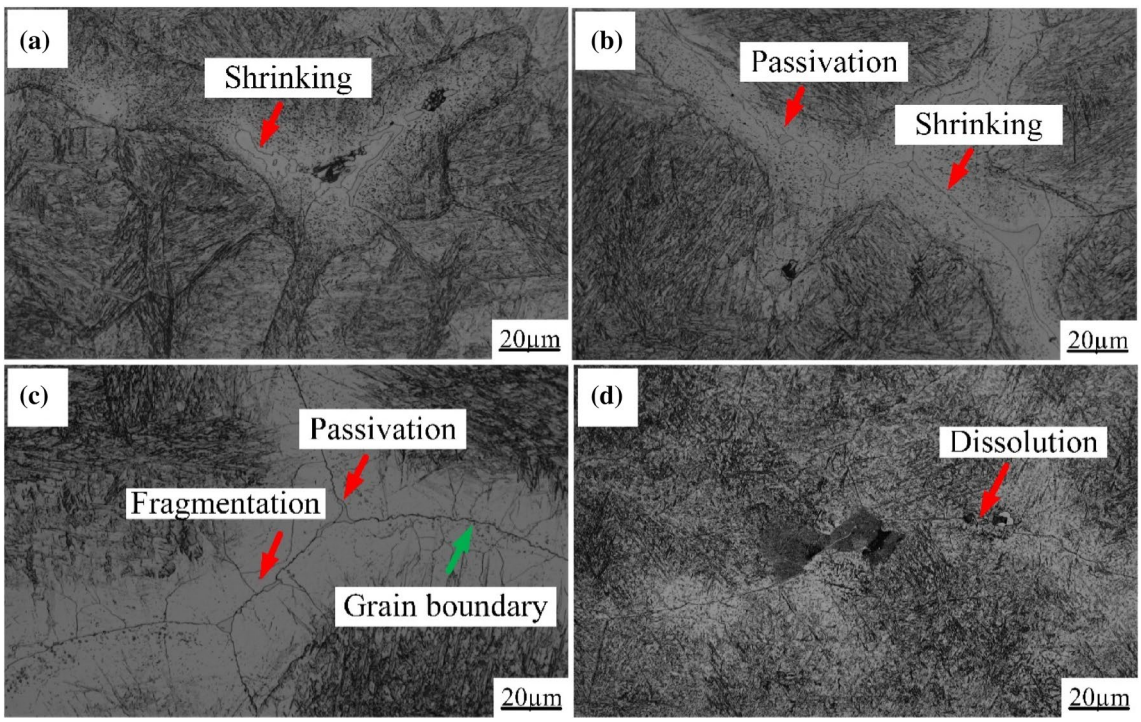

Fig. 6 Primary carbide morphologies at different homogenisation temperature for 30 min: **a** 1100 °C; **b** 1150 °C; **c** 1200 °C and **d** 1230 °C

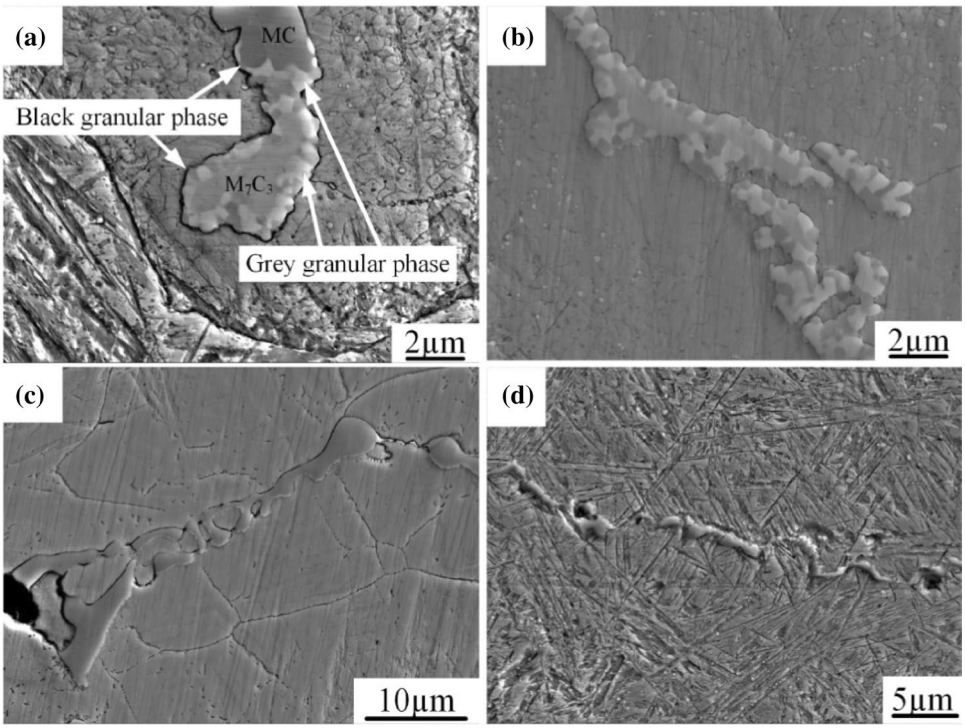

Fig. 7 Secondary electron images of primary carbide in QUANTA 600 scanning electron microscope (SEM) at different homogenisation temperature for 30 min: **a** 1100 °C; **b** 1150 °C; **c** 1200 °C and **d** 1230 °C

interfaces of MC/γ and M_7C_3/γ, respectively. The black and grey granular phases gradually grew up and connected, separating the primary carbide from the γ matrix when the temperature increased from 1100 to 1150 °C. Nevertheless, such characteristics were disappeared when the temperature was 1200 and 1230 °C. The primary carbides got partial dissolution and presented a discontinuous state. As a representative, the elemental scanning maps of primary carbides at temperature of 1100 °C are revealed in Fig. 8. The colours in the maps are correlated with the elemental concentration.

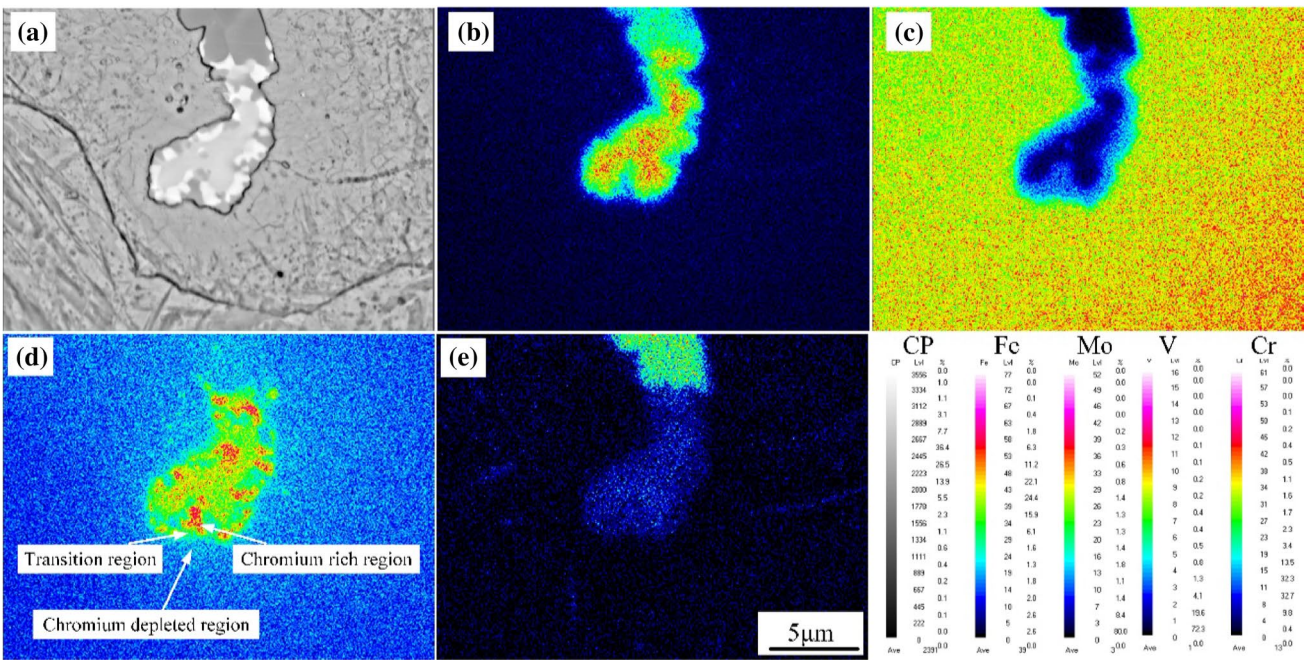

Fig. 8 Elemental scanning maps of primary carbides under homogenised state in QUANTA 600 scanning electron microscope (SEM) at the temperature of 1100 °C for 30 min: **a** backscatter image; **b** Mo; **c** Fe; **d** Cr and **e** V

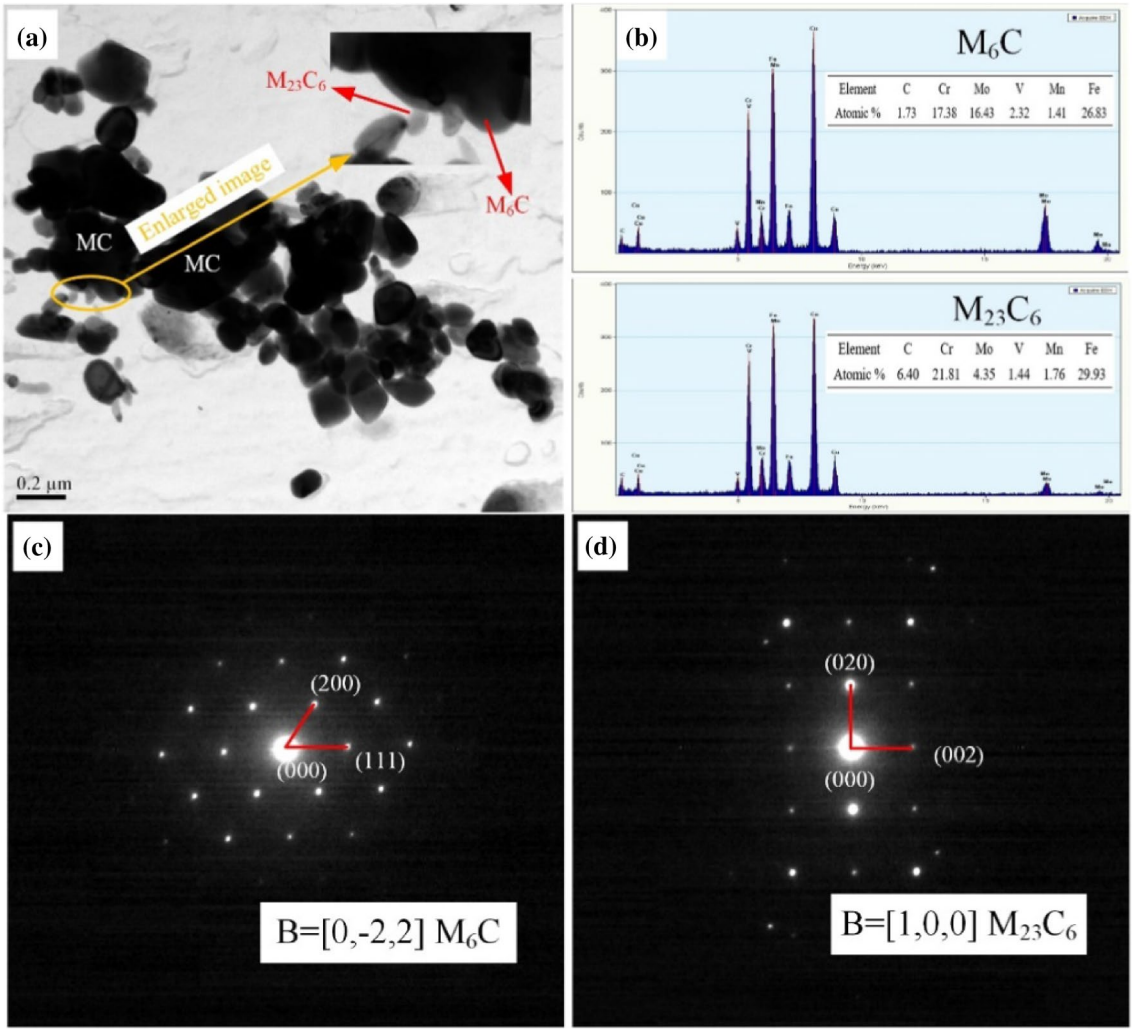

Fig. 9 **a** TEM image after homogenisation treatment at 1100 °C for 30 min and corresponding: **b** EDS analysis results of granular phase in decomposition zone; SAED patterns of **c** M_6C and **d** $M_{23}C_6$

The elemental concentration variation corresponds to the formation of black and grey granular phase in the decomposition zones of primary carbides (Fig. 8). TEM images and the corresponding SAED patterns are listed in Fig. 9, together with the chemical composition of the black and grey granular phase in the decomposition zone. The morphology of primary carbide presents a broken state owing to its large size during the carbon replication process. The granular phases are observed around the primary carbide MC, which is revealed in the enlarged image in Fig. 9a. The EDS analysis results of granular phases are listed in Fig. 9b. Copper appears in the spectra due to the presence of copper mesh. The new granular phases contain high contents of Cr and Mo, whose crystal structure is $M_{23}C_6$ and M_6C, respectively. Moreover, the formation of granular carbides consumes a mass of Cr atoms, and the required Cr atoms are transported from the adjacent matrix phase. Consequently, the Cr-rich region, transition region and depleted region are detected in Fig. 8d. The elemental scanning maps of primary carbides in Fig. 7c at temperature of 1200 °C are revealed in Fig. 10. There is no concentration variation in primary carbide MC, indicating the decomposed carbide phase has completely dissolved. A bulk of primary carbides gradually dissolved into the γ matrix, and the microstructure surrounding the primary carbides was more distinct when the homogenisation temperature increased. Furthermore, the primary carbide M_7C_3 almost dissolved into the γ matrix at 1200 °C, marked by the red circle in Fig. 10a.

Figure 11 shows the changes of interdendritic dot-like carbide at different homogenisation temperatures. The number of dot-like carbides decreases sharply with the increase of temperature. The dot-like carbides far from the grain boundary mostly dissolved, and those on the grain boundary still existed when the homogenisation temperature increased

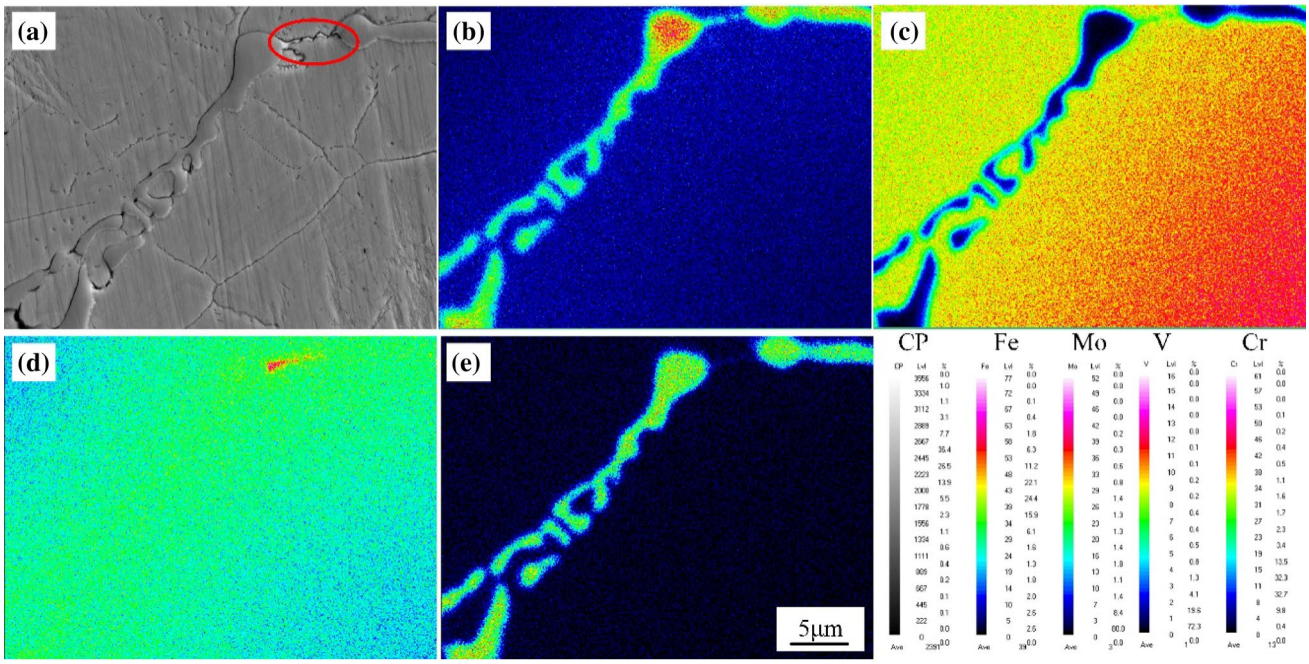

Fig. 10 Elemental scanning maps of primary carbides under homogenised state in QUANTA 600 scanning electron microscope (SEM) at the temperature of 1150 °C for 30 min: **a** backscatter image; **b** Mo; **c** Fe; **d** Cr and **e** V

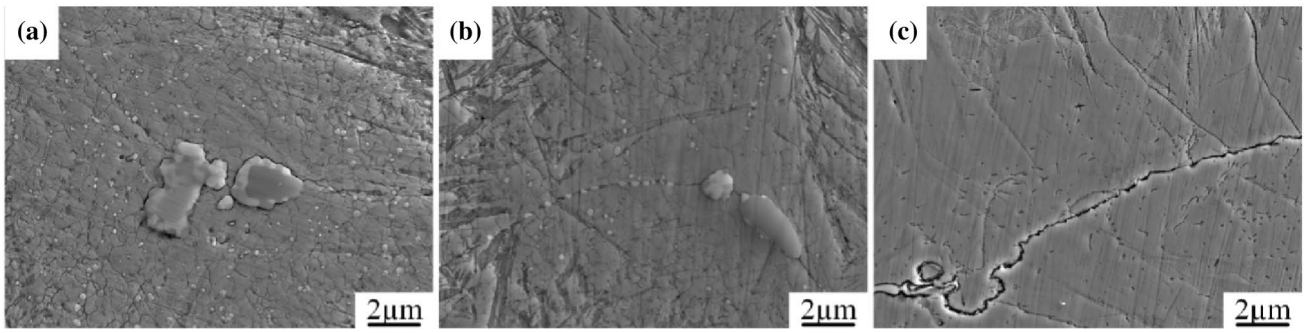

Fig. 11 Interdendritic dot-like carbide changes in QUANTA 600 scanning electron microscope (SEM) at **a** 1100 °C; **b** 1150 °C and **c** 1200 °C

to 1150 °C. Afterwards, the dot-like carbides gradually dissolved into the matrix when the temperature increased to 1200 °C. Finally, there was almost no existence of dot-like carbides in the interdendritic region at 1200 °C.

3.4 Microhardness

Hardness is the comprehensive ability of a solid material to resists elastic deformation, plastic deformation and fracture. Due to the solution strengthening and the presence of primary carbide, microhardness is sensitive to chemical element heterogeneity based on the same matrix. Microhardness is measured by the size of indentation and the microhardness between dendrite arm and interdendrite should be changeable at different homogenisation temperatures. Figure 12 shows the variation of the average microhardness values and the corresponding standard deviation values of the homogenised specimens; the standard deviation values represent the hardness homogeneity. With the increase of homogenisation temperature, the grains were coarsening, the average microhardness value gradually decreased from 841 to 650 HV. Nevertheless, the standard deviation value decreased first and then increased, which met the minimum 32 HV at a homogenisation temperature of 1200 °C, indicating that hardness homogeneity was the best at a homogenisation temperature of 1200 °C. The high-temperature homogenisation treatment promoted the diffusion of chemical elements and reduced the difference in elemental

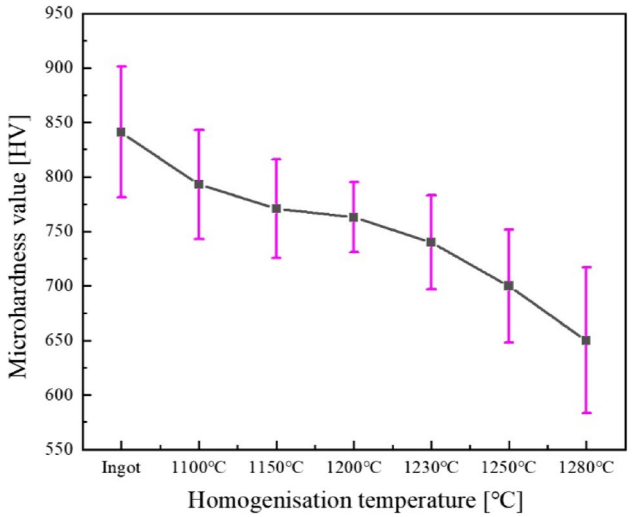

Fig. 12 Microhardness of samples after different homogenisation temperatures

concentration, thus increasing the hardness homogeneity. Overheating appeared at a homogenisation temperature of 1230 °C. Additionally, the solute redistribution in the local melting area caused the segregation again when the homogenisation temperature exceeded 1250 °C.

4 Discussion

4.1 Relationship between Dendrite Segregation and Solidus Temperature

According to the equilibrium solidification path [23], the liquidus temperature and solidus temperature of H13 steel are 1454 and 1315 °C. However, because of the presence of dendrite segregation in as-cast H13 steel, the liquidus temperature and solidus temperature in dendrite segregation region were not in correspondence with the temperatures mentioned above [24]. According to the computational formula of solidus temperature [25], the variation of practical solidus temperature can be predicted.

$$T_s = T_0 - \sum_{1}^{n} m_i[\%i] \tag{2}$$

where T_s is the solidus temperature, T_0 is the melting point of pure iron, i is the chemical element that affects solidus temperature, $[\%i]$ is the mass fraction of chemical element i, m_i is the influence coefficient of the chemical element i and n is the number of chemical elements that affect the solidus temperature. According to the formula, the solidus temperature varies with the chemical element types and contents. However, Eq. (2) is an empirical formula, the accuracy of calculated results is not clear. The solidus temperature can also be calculated using the JMatPro V9.0 software [26]. The mass fraction distribution of chemical elements in the interdendritic region are plotted in Fig. 13a. The solidus temperature of the matrix at different locations in the interdendritic region is calculated and plotted in Fig. 13b. The zero point represents the interface between the liquation carbide (primary carbide) and the matrix, the negative value indicates that the point is located on the left side of the liquation carbide and the positive value is on the right side of the liquation carbide. The solidus temperature of the matrix around the interdendritic liquation carbide presented a W type, which varied from 1230 to 1390 °C and decreased largely in comparison with the equilibrium state. When the alloying element content was higher, the solidus temperature

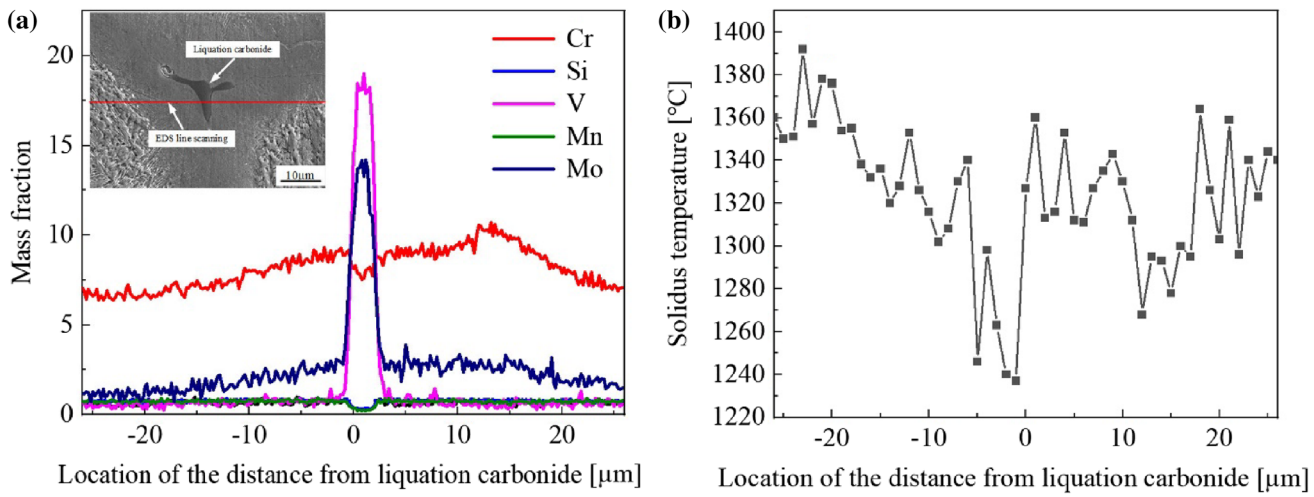

Fig. 13 **a** Mass fraction variation of elements around primary carbide and **b** solidus temperature around primary carbide

was lower. When the homogenisation temperature exceeded 1230 °C, local melting appeared.

4.2 Evolution Mechanism of Primary Carbides

Understanding the primary carbide evolution in the Cr–Mo–V steel is essential to heat treatment and thermo-mechanical working. During non-equilibrium solidification of H13 steel, the primary carbide formed directly from the liquid phase, whose chemical element content was higher than that in neighbouring matrix phase and the dissolution temperature range of these primary carbides was largely extended. As illustrated by Wang et al. [12], the segregation of solute elements promotes the formation of primary carbides during solidification. Therefore, in the dendrite segregation region of as-cast H13 steel, the mass fraction of non-metallic elements is assumed to enlarge two times and the metallic elements enlarge three times, except Cr (enlarging two time as well) due to its better diffusion ability. Based on the assumed compositions, the relationship between carbide and temperature in the dendrite segregation region was calculated by Thermo-calc software as plotted in Fig. 14. The primary carbides M_7C_3 and MC gradually dissolved when the temperature was over 900 °C, and they completely dissolved at about 1400 °C. The secondary $M_{23}C_6$ started to form at about 900 °C, corresponding to the decomposition of primary carbides. From the point of solidification, the primary carbides M_7C_3 and MC directly formed the liquid phase at about 1400 °C.

In as-cast H13 steel, both of the thermodynamic and kinetic conditions need to be met for carbide formation and decomposition during the subsequent heating [12]. Owing to the rapid cooling rate during solidification, there were no sufficient kinetic conditions for the complete transformation of primary carbide. Finally, an amount of metastable carbides (M_7C_3 and MC) were remnant at room temperature. During the subsequent reheating, the metastable primary carbides decomposed and dissolved when the temperature exceeded 900 °C. The primary carbide in

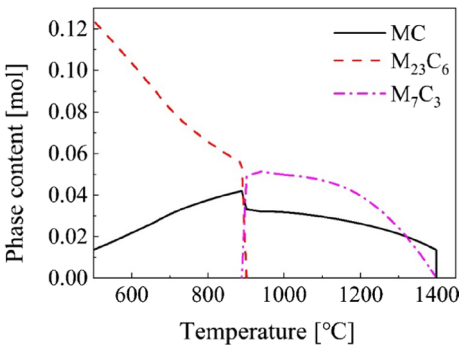

Fig. 14 Calculation results of carbide phase in H13 steel

as-cast H13 steel belongs to the multi-component phase, where Cr, Mn, Mo and V have a large solubility. According to Hudd [27], the solid solution product formula of binary phase can still be applied to multi-component MC_x phase, where M is an alloying component and x is the stoichiometric number. The solid solution product formula can be interpreted as follows:

$$\log \frac{[M][C]}{x} = A - B/T \tag{3}$$

where A and B are the corresponding constants in the solution product formula. The stoichiometric number x will change with the chemical composition and system temperature. That is to say, the chemical formula of the MC_x phase is not constant over a large range. Furthermore, the solubility of the corresponding chemical components of the multi-component phase in the iron matrix is smaller than that of the less-component phase due to the mixing entropy [28, 29]. Therefore, the multi-component primary carbides prefer to decompose into the less-component primary carbides rather than dissolve directly at an elevated temperature.

Vanadium is a strong carbide-forming element; Cr and Mo are the weak carbide-forming elements. For example, V strongly promotes the formation of MC-type carbides, but Cr and Mo weaken the binding force of chemical bond [30]. Primary MC carbides in the alloys tend to decompose into more stable carbides, like $M_{23}C_6$ [31]. Moreover, the evolution process of primary carbide is affected by the partition of alloying elements between carbide and the γ phase. Previous work had demonstrated the transformations [32, 33]:

$$MC + \gamma \rightarrow M_{23}C_6 + M_6C \tag{4}$$

$$M_7C_3 + \gamma \rightarrow M_6C \tag{5}$$

The decomposition process of primary carbide MC_x can be interpreted as follows. When MC_x began to decompose due to the presence of concentration gradient, MC_x provided C, V and Mo, while the γ matrix adjacent to MC_x mainly provided Cr. The reactions proceeded when the thermodynamic and kinetic conditions were satisfied, i.e.

$$23M + 6C \rightarrow M_{23}C_6 \tag{6}$$

$$6M + C \rightarrow M_6C \tag{7}$$

The new carbide phase ($M_{23}C_6$ and M_6C) formed at the interface of MC_x/γ, whose nucleation and growth consumed a large number of Cr in the γ matrix, leading to the appearance of a Cr-depleted region adjacent to MC_x. There was also a difference in Cr content between $M_{23}C_6$ and M_6C. Referring to the movement of Cr atoms between γ

matrix and carbide, the formation of carbide in decomposition zone around the primary carbide was that M_6C firstly formed with lower Cr content, which preferentially met the thermodynamics condition for nucleation. Through diffusion, $M_{23}C_6$ generated at the M_6C/γ interface with minimal energy consumption. The diffusion of atoms and the dissolution of the carbide phase proceeded anytime. The concentration gradient between the primary carbide and γ matrix gradually declined because the atoms diffused a short distance. With the progress of homogenisation at a higher temperature, the decrease of concentration gradient lowered the phase transformation driving force; there were insufficient kinetics for nucleation and growth of carbide. Therefore, the decomposition zone around the primary carbide was limited and gradually disappeared.

4.3 Microhardness Analysis

In general, the microhardness of as-cast H13 steel is affected by solid solution, precipitation and dislocation. The contribution from the interstitial elements carbon and nitrogen to the solid solution strengthening was thought to be negligibly small [34]. When alloying solute atoms dissolve into the solvent lattice, the size mismatch between alloying solute atoms and the host material lattice allows lattice distortion to take place, that is, the solvent atoms adjacent to alloying solute atoms will deviate from their equilibrium position. When the lattice distortion is larger, the lattice is more unstable. Similarly, when there are more alloying solute atoms, the lattice distortion energy per unit volume will be greater. In solidification structure of H13 steel, the dendrite arm can be defined as sub-supersaturated solid solution and the interdendrite can be supersaturated solid solution. The crystal lattice of the matrix in supersaturated solid solution region was more distorted than that in sub-supersaturated solid solution region after the formation of a solid solution, resulting in a larger lattice distortion. The lattice distortion changes the lattice constant; different lattice distortion means different distances and different binding forces between atoms. The primary carbides also formed directly from the liquid phase in the supersaturated solid solution region. Therefore, the supersaturated solid solution region had the higher hardness values than those in sub-supersaturated solid solution region. The XRD spectra of three homogenised state specimens (ingot, homogenised at 1100 °C and homogenised at 1200 °C) and the corresponding analysis results are illustrated in Fig. 15. The retained austenite peak was initially visible in non-homogenised ingot, and the peak disappeared when the ingot was homogenised at 1100 and 1200 °C (Fig. 15a). Similarly, stability of under-cooled austenite

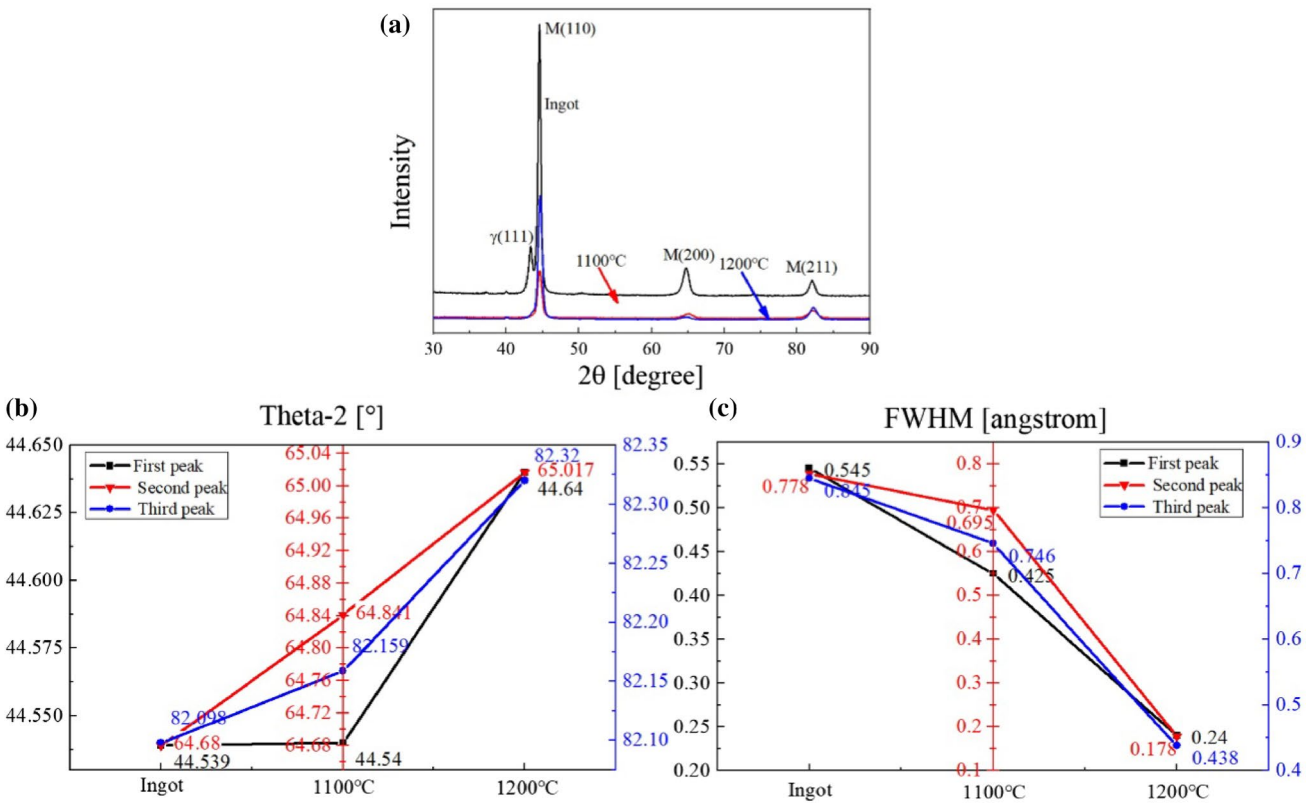

Fig. 15 XRD analysis results of H13 steel under different homogenised states: **a** spectra; **b** theta-2 and **c** FWHM

decreased after homogenisation. Figure 15b presents the changes of diffraction peak angle under different homogenised state, among which the black scatter line corresponds to the left vertical axis highlighted by black colour, the red scatter line corresponds to the middle vertical axis highlighted by red colour and the blue scatter line corresponds to the right vertical axis highlighted by blue colour. The three peak diffraction angles (theta-2) were 44.539°, 64.680° and 82.098° for samples non-homogenised, 44.540°, 64.841° and 82.159° for samples homogenised at 1100 °C and 44.640°, 65.017° and 82.320° for samples homogenised at 1200 °C. During homogenisation, the solute atoms diffused in a short distance. Consequently, the lattice constants and chemical composition of the matrix were changeable, which was reflected by the variation of the diffraction angle [35]. The XRD peaks in Fig. 15b all shift to the right, indicating that the lattice constants slightly decreased [36] and the chemical composition changed. Meanwhile, microstructural observations show that a more uniform matrix was obtained with the increase of homogenisation temperature. Accordingly, the two perspectives on the results come with a high degree of complementarity. The full width at half maximum (FWHM) of H13 steel under different homogenised states is described in Fig. 15c; the method of data presentation is the same with Fig. 15b. As proposed by Bouras et al. [37], the XRD peak broadening is directly related to the structural heterogeneity; a more uniform matrix structure is reflected by the reduction of FWHM of matrix peaks. The FWHM gradually decreased with the increase of homogenisation temperature, indicating that a more uniform matrix composition was obtained.

5 Conclusion

The as-cast H13 steel used in this work was prepared by vacuum induction melting in the laboratory, the effect of homogenisation temperature range on the microstructure evolution and microhardness of as-cast H13 steel was studied during homogenisation.

1. In as-cast H13 steel, the segregation of alloying elements of chromium, molybdenum and vanadium occurred in the interdendritic regions, and metastable primaryM_7C_3 and MC directly formed in the liquid phase, part of which remained unchanged during the subsequent cooling process and also maintained a stable state at room temperature.
2. The experimental results showed that the optimised homogenisation temperature range was from 1150 to 1230 °C, which agreed with the theoretical calculation. Alloying element segregation lowered the solidus temperature; the solidus temperatures around the primary carbide presented a W type. The grain boundary bulged and initiated local melting in the segregation region when the homogenisation temperature exceeded 1230 °C. The primary carbide underwent shrinking, passivation, fragmentation and dissolution in the final stage. Secondary carbide $M_{23}C_6$ and M_6C formed at the interface of MC/γ and M_7C_3/γ at 1100 and 1150 °C. Primary carbide (M_7C_3) and secondary carbide ($M_{23}C_6$ and M_6C) dissolved into the matrix when the temperature increased to 1200 °C.
3. When the homogenisation temperature increased from 1150 to 1230 °C, the microhardness value decreased from 841 to 740 HV and the standard deviation microhardness gradually decreased from 60 to 43 HV, indicating the microhardness homogeneity around the dendrite segregation region increased. When the homogenisation temperature exceeded 1230 °C, the standard deviation microhardness increased, and the microhardness homogeneity worsened due to the overburning and overheating.

Acknowledgements This work was supported by the National Key Research Project of China (2016YFB0300402).

References

1. L.A. Norstrom, L. Jonson, B. Klarenfjord, Die Cast. Manag. **24**, 12 (1990)
2. A. Persson, *On Tool Failure in Die Casting* (Uppsala University, Uppsala, 2003), p. 7
3. K.D. Fuchs, Hot-work tool steels with improved properties for die casting applications, in *Proceedings of the 6th International Tooling Conference*, Karlstad, Sweden, 10–13 September 2002 (Karlstad Univ., Karlstad, 2002), pp. 17–26
4. NADCA #207–2003 (North American Die Casting Association, Illinois, 2003)
5. M. Torkar, F. Vodopivec, S. Petovar, Mater. Sci. Eng. A **173**, 313 (1993)
6. H. Wang, K. Xu, S. Lu, in The 6th Baosteel Biennial Academic Conference, Shanghai (2015)
7. S. He, C.S. Li, J.Y. Ren, Y.H. Han, Steel Res. Int. **89**, 1800148 (2018)
8. M.H. Lu, Y.Y. Tian, H.Y. Cai, G.H. Yin, Heat Treat. Met. **35**, 9 (2010)
9. Y.H. Han, C.S. Li, J.Y. Ren, C.L. Qiu, Y.Q. Zhang, J.Y. Wang, ISIJ Int. **59**, 1893 (2019)
10. T. Okuno, Trans. ISIJ. **27**, 51 (1987)
11. A.G. Ning, H.J. Guo, X.C. Chen, X.L. Sun, J. Univ. Sci. Technol. B. **36**, 895 (2014)
12. H. Wang, J. Li, C.B. Shi, J. Li, B. He, Mater. Trans. **58**, 152 (2017)
13. W.W. Song, Y.A. Min, X.C. Wu, Trans. Mater. Heat Treat. **30**, 122 (2009)
14. K.E. Thelning, *Steel and Its Heat Treatment* (Butterworth, London, 2013)
15. B. Bryson, W.E. Bryson, *Heat Treatment, Selection, and Application of Tool Steels* (Hanser Gardner Publications, Cincinnati, 2005)
16. ASM International, *ASM Handbook Volume 4, Heat Treating* (American Society for Metals, Metals Park, 2006)

17. Y. Xie, G. Cheng, X. Meng, Y. Huang, Metall. Res. Technol. **114**, 206 (2017)
18. M. Wang, D.S. Ma, Z.T. Liu, H.X. Chi, J.Q. Dai, Heat Treat. Met. **39**, 5 (2014)
19. M.T. Mao, H.J. Guo, X.L. Sun, F. Wang, X.C. Chen, J. Guo, Chin. J. Eng. **39**, 1174 (2017)
20. M.R. Ghomashchi, C.M. Sellars, J. Met. Sci. **18**, 44 (2013)
21. J. Guo, L.Q. Ai, T.T. Wang, Y.L. Feng, D.C. Wan, Q.X. Yan, Mater. Sci. Eng. A **715**, 359 (2018)
22. Ch.A. Gandin, M. Rappaz, D. West, B.L. Adams, Metall. Mater. Trans. A **26**, 1543 (1995)
23. Y.J. Lin, K.M. McHugh, Y.Z. Zhou, E.J. Lavermia, Metall. Mater. Trans A **38**, 1632 (2007)
24. Y. Meng, B.G. Thomas, Metall. Mater. Trans B **34**, 685 (2003)
25. J.X. Chen, *Chart Data Manual for Steelmaking*, 2nd edn. (Metallurgical Industry Press, Beijing, 2010), p. 510
26. J.G. Chen, X.L. Xing, Y.J. Wang, Y.F. Zhou, X.J. Ren, Y.L. Yang, Q.X. Yang, J. Mater. Eng. Perform. **24**, 1157 (2015)
27. R.C. Hudd, A. Jones, M.N. Kale, J. Iron Steel Res. Int. **209**, 121 (1971)
28. F. Otto, Y. Yang, H. Bei, E.P. George, Acta Mater. **61**, 1628 (2013)
29. L.C. Tsao, C.S. Chen, C.P. Chu, Mater. Design **36**, 854 (2012)
30. X.Z. Qin, J.T. Guo, C. Yuan, J.S. Hou, L.Z. Zhou, H.Q. Ye, Acta Metall. Sin. **46**, 213 (2010)
31. H.M. Tawancy, N.M. Abbas, A.I. Al-Mana, T.N. Rhysjones, J. Met. Sci. **29**, 2445 (1994)
32. X. Xiao, C. Zeng, J.S. Hou, X.Z. Qin, J.T. Guo, L.Z. Zhou, Acta Metall. Sin. **50**, 1031 (2014)
33. X.L. Wu, G.N. Chen, J. Mater. Sci. **34**, 3355 (1999)
34. P.A. Korzhavyi, R. Sandström, Mater. Sci. Eng. A **626**, 213 (2015)
35. C. Li, J.C. Li, M. Zhao, Q. Jiang, J. Alloy. Compd. **475**, 752 (2009)
36. Y. Liu, M. Chen, Y.X. Li, X. Chen, Rare Metal Mat. Eng. **38**, 1602 (2009)
37. M. Bouras, A. Boumaiza, V. Ji, N. Rouag, Theor. Appl. Fract. Mec. **61**, 51 (2012)